### **Research Article**

Mustafa Abbas Fadhel, Adnan Asghar, Liaquat Ali Lund, Zahir Shah\*, Narcisa Vrinceanu\*, and Vineet Tirth

# Dual numerical solutions of Casson SA-hybrid nanofluid toward a stagnation point flow over stretching/shrinking cylinder

https://doi.org/10.1515/ntrev-2023-0191 received June 14, 2023; accepted December 21, 2023

Abstract: A computational study of Casson sodium alginatehybrid nanofluid of stagnation point flow through a shrinking/stretching cylinder with radius effect was carried out. Since the hybrid nanofluid is considered more contemporary type of nanofluid, it is currently being employed to enhance the efficiency of heat transmission rates. The aim of this study is to scrutinize the effect of particular parameters, such as the shrinking parameter, the Reynold number, the Casson fluid parameter, the solid copper volume fraction, and the Prandtl number, on the temperature and velocity profiles. Furthermore, the research looked into the variation of skin friction coefficient as well as the Nusselt number according to the Casson fluid parameters, and the copper solid volume fraction against shrinking parameter was investigated as part of this study. By including the appropriate similarity variables in the alteration, the nonlinear partial differential equation has been transformed into a set of ordinary differential equations (ODEs). In the end, the MATLAB bvp4c solver program is used to rectify ODEs.

Mustafa Abbas Fadhel: Mathematics Department, College of Education for Pure Sciences, University of Al-Muthanna, Samawa, 66001, Iraq Adnan Asghar: School of Quantitative Sciences, UUM College of Arts & Sciences, Universiti Utara Malaysia, UUM Sintok, Kedah Darul Aman, Malaysia

**Liaquat Ali Lund:** KCAET Khairpur Mir's, Sindh Agriculture University, Tandojam Sindh, 70060, Pakistan

**Vineet Tirth:** Mechanical Engineering Department, College of Engineering, King Khalid University, Abha, 61421, Asir, Saudi Arabia; Research Center for Advanced Materials Science (RCAMS), King Khalid University, Guraiger, Abha, 61413, Asir, Saudi Arabia

The findings revealed the existence of two solutions for shrinking surface with varying copper volume fractions and Casson fluid parameter values. Furthermore, the temperature profile rate was reduced in both solutions as the strength of the Reynold number, Casson fluid parameter, and copper volume fraction increased. Finally, non-unique solutions were obtained in the range of  $\lambda \geq \lambda_{ci}$ .

**Keywords:** SA-hybrid nanofluid, dual solutions, stretching/shrinking cylinder, stagnation point

# 1 Introduction

The investigation of fluid flow and heat transmission formed by way of a stretching/shrinking sheet has many applications in industry, including thermal insulation, the production of synthetic materials and glass, the transportation of underground species, the drying of porous materials, the regeneration of oil, and solar thermal devices. Heat exchange and flow exploration are the key industrial applications, and they are critical success factors since the quality of the finished produced product is based on the rate of convection heat exchange as well as the velocity gradient coefficient [1–8].

Hybrid nanofluids, which contain dual sorts of nanoparticles spread in a common fluid, are an example of more sophisticated nanofluids. Because of its potential to advance the temperature transmission rate related to regular nanofluids, the study of temperature transmission in a hybrid nanofluid has garnered substantial prior exploration. This has led to the widespread notion that hybrid nanofluids are the ideal temperature transmission fluids for use in a wide variety of electronics, inverter cooling, and manufacturing applications. Hayat and Nadeem [9] described the moment of thermal flow in a hybrid radiative nanofluid with a heat source over a rotational plate. They came to the conclusion that the heat transfer rate of hybrid nanofluid is greater than that of normal nanofluid

<sup>\*</sup> Corresponding author: Zahir Shah, Department of Mathematical Sciences, University of Lakki Marwat, Lakki Marwat 28420, Khyber Pakhtunkhwa, Pakistan, e-mail: Zahir@ulm.edu.pk

<sup>\*</sup> Corresponding author: Narcisa Vrinceanu, Department of Industrial Machines and Equipments, Faculty of Engineering, "Lucian Blaga" University of Sibiu, 10 Victoriei Boulevard, Sibiu, Romania, e-mail: vrinceanu.narcisai@ulbsibiu.ro

Mustafa Abbas Fadhel *et al.* 

with occurrence of heat generation, radiation, and chemical reaction. Waini *et al.* [10] conducted research that resulted in the development of a numerical simulation for hybrid nanofluid flow through a perpendicular surface containing a permeable medium. Gholinia *et al.* [11] examined a mathematical solution to the problem of a hybrid nanofluid moving past a porous stretched cylinder. Some more studies have lately concentrated on a distinct sort of hybrid nanofluid heat transfer and flow mechanism in previous studies [12–16].

Now, a non-Newtonian fluid known as sodium alginate (SA) has gained considerable attention due to its many biological and industrial applications, such as paper manufacture, textiles, products for the food service industry, and tissue making. Hatami and Ganji [17] conducted a study that resulted in the development of numerical and analytical approaches for SA-based nanofluid thermal transport and flow modeling. Akinshilo et al. [18] investigated the different flow and heat transfer effects that were caused by SA-based nanofluids. Besides, Hussanan et al. [19] investigated the influence of a non-magnetic and magnetized nanoparticles combination on an SA-based hybrid nanofluid as it passed via a stretched/diminishing sheet. They revealed that SA-based hybrid nanofluids have a faster heat dispersion ratio than water-based hybrid nanofluids. Hammachukiattikul et al. [20] explored the SA-based hybrid nanofluid by a heat source, radiation, and inclined Lorentz force impacts over a diminishing/stretch layer. Dawar et al. [21] investigated the SA-based hybrid nanofluid with the combination of copper and alumina particles magnetized heterogeneously close to a convectively warmed layer of a stretch curved geometry. Further studies on SA-hybrid nanofluid were carried out by deploying various fluid flow models [22-24].

A considerable number of scholars have taken into consideration the problem of stagnation point flow in the direction of a cylinder. Wang [25] took into consideration the stagnation flow that was flowing approaching a circular cylinder. Wang [26] developed this problem further by taking into consideration a partial factor condition on the surface of the cylinder. Reddy Gorla [27] investigated a problem that Wang [25] had also encountered, but he focused on how the Prandtl numbers affected the heat transmission rate. Merkin et al. [28] examined the flow of stagnation point as well as heat transport in a cylinder that was exponentially stretching and diminishing. Zaimi et al. [29] investigated the impact of drag on flow of unsteady through a diminishing cylinder and discovered that dual solutions happen for a given range of unsteadiness and suction parameters. Cunning et al. [30] looked into the impact of transpiration and rotational on the stagnation

flows approaching a circular cylindrical. Moreover, Soomro *et al.* [31] studied that nanofluids flow through a permeability-diminishing vertical cylinder including slip condition. Lok and Pop [32] explored this problem in this regard by taking into account the stagnation point flows and suction impacts. Waini *et al.* [33] examined the stagnation point on a stretch/diminishing cylinder for a hybrid nanofluid. More relevant analyses to model the flow across a cylinder under various parameters can be seen in the literature studies [34–38].

The stagnation point flow through a stretching/shrinking cylinder for water-based hybrid nanofluid was studied by Waini *et al.* [33] without taking the Casson fluid parameter into consideration. However, the suggested problem seeks to fill in the gaps mentioned by Waini *et al.* [33] by examining the impact of the Casson fluid parameter for SA–hybrid nanofluid. Consequently, for this study, a novel physical structure of SA–hybrid nanofluid to a stagnation point flow across the stretching/shrinking cylinder with Casson fluid parameter was developed.

This simulation examines the interactions of hybrid nanofluids while taking the solid volume fractions of the nanoparticles into consideration. The hybrid nanofluid is studied in this research by suspending two distinct nanoparticles: Al<sub>2</sub>O<sub>3</sub> (alumina) and Cu (copper), in SA. This study takes into account the Reynolds number, shrinking surface, Casson fluid, the solid volume fraction of copper, and Prandtl number parameters presented in velocity and temperature profiles behavior. In addition to the investigation of the local skin friction and the Nusselt number versus the Casson fluid parameters, the copper solid volume fraction was also studied. A comparison with the results already available in the pertinent research literature was made to express the reliability of the generated numerical results. The authors assured that the findings are original and have not been taken into account by any other studies before.

# 2 Mathematical formulation

In Figure 1, we consider a hybrid nanofluid of Casson-based flowing for a flow of stagnation point over a stretching/shrinking cylinder of radius a. The polar coordinates of a cylinder are written as (z,r), where z is the axial direction and r is the radial direction. The stagnation line is located at z=0 and r=a, and the flow is assumed to be axisymmetric about the z-axis. When b=0, the cylinder is at rest; when b>0 or b<0, the cylinder is stretched or shrunk, and the surface velocity is given by  $w_w(z)=2bz$ . Meanwhile, we

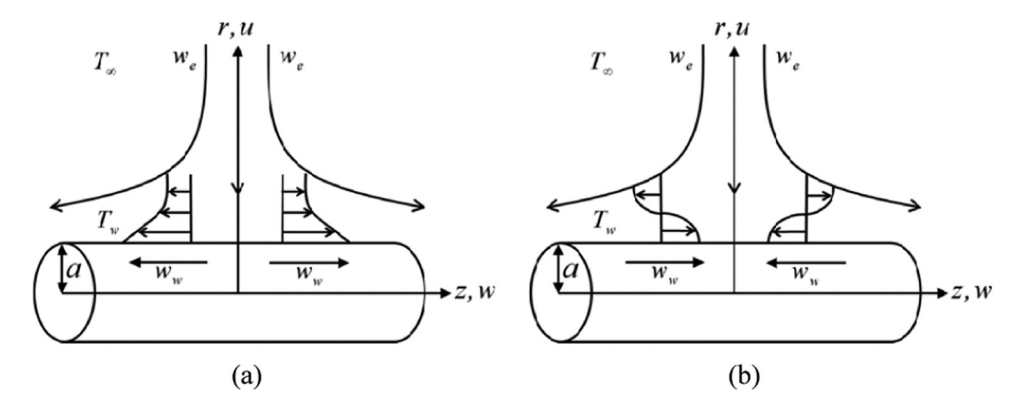


Figure 1: Geometry of the problem: (a) stretching cylinder and (b) shrinking cylinder.

define  $w_{\rm e}(z)=2cz$  for cases where c>0 to represent the free stream velocity. In addition,  $T_{\rm w}>T_{\infty}$  holds true, indicating that temperature of the surface  $(T_{\rm w})$  is always greater than the ambient temperature  $(T_{\infty})$ . Since the hybrid nanofluid is a stable composite, it is presumed that the nanoparticle has a spherical shape and is of uniform size. Agglomeration is neglected. Therefore, the equations (Wang [26], Lok and Pop [32]) that regulate the flow of the hybrid nanofluid are as follows:

$$\frac{\partial(rw)}{\partial z} + \frac{\partial(ru)}{\partial r} = 0,\tag{1}$$

$$w\frac{\partial w}{\partial z} + u\frac{\partial w}{\partial r} = w_{\rm e}\frac{\mathrm{d}w_{\rm e}}{\mathrm{d}z} + \frac{\mu_{\rm hnf}}{\rho_{\rm hnf}} \left[ 1 + \frac{1}{\beta} \right] \left\{ \frac{\partial^2 w}{\partial r^2} + \frac{1}{r} \frac{\partial w}{\partial r} \right\},\tag{2}$$

$$w\frac{\partial T}{\partial z} + u\frac{\partial T}{\partial r} = \frac{k_{\text{hnf}}}{(\rho c_{\text{n}})_{\text{hnf}}} \left\{ \frac{\partial^2 T}{\partial r^2} + \frac{1}{r} \frac{\partial T}{\partial r} \right\}, \tag{3}$$

with boundary conditions:

$$\begin{cases} u = 0, w = w_{\text{w}}, T = T_{\text{w}} \text{ at } r = a \\ w \to w_{\text{e}}, T \to T_{\text{o}} \text{ at } r \to \infty \end{cases}$$
 (4)

where u and w stand for the r and z components of the velocity, respectively, and T is the temperature of the nanofluid. Additionally, Table 1 defines the thermophysical

parameters of the hybrid nanofluid. Table 2 lists the physical characteristics of  $Al_2O_3$ , Cu, and SA. Here, we have the volume fractions of  $Al_2O_3$  (represented by  $\phi_{Al_2O_3}$ ) and Cu (represented by  $\phi_{Cu}$ ). The fluids, nanofluids, and hybrid nanofluids are presented by the subscripts f, nf, and hnf, respectively.

The appropriate transformations are as follows:

$$\begin{cases} u = \frac{-caf(\eta)}{\sqrt{\eta}}, w = 2czf'(\eta) \\ \theta(\eta) = \frac{T - T_{\infty}}{T_{W} - T_{\infty}}, \eta = \left(\frac{r}{a}\right)^{2} \end{cases}$$
 (5)

Using these definitions (5), we find that equation (1) holds true. In addition, equation (5) is a similarity

Table 2: Thermophysical properties of SA, Cu, and Al<sub>2</sub>O<sub>3</sub>

Properties	SA	Cu	$Al_2O_3$
$\rho(\text{kg/m}^3)$	989	8,933	3,970
$c_{\rm p}({\rm J/kg~K})$	4,175	385	765
k(W/m K)	0.6376	400	40
Pr	7	_	_

Table 1: Thermophysical properties of hybrid nanofluid

Properties	Hybrid nanofluid
Dynamic viscosity	$\mu_{\rm hnf} = \frac{\mu_{\rm f}}{(1 - \phi_{\rm Cu})^{2.5} (1 - \phi_{\rm Al_2O_3})^{2.5}}$
Density	$\rho_{\rm hnf}/\rho_{\rm f} = (1 - \phi_{\rm Cu})[(1 - \phi_{\rm Al_2O_3}) + \phi_{\rm Al_2O_3}\rho_{\rm Al_2O_3}/\rho_{\rm f}] + \phi_{\rm Cu}\rho_{\rm Cu}/\rho_{\rm f}$
Thermal conductivity	$k_{\rm hnf} = \frac{k_{\rm Cu} + 2k_{\rm nf} - 2\phi_{\rm Cu}(k_{\rm nf} - k_{\rm Cu})}{k_{\rm Cu} + 2k_{\rm nf} + \phi_{\rm Cu}(k_{\rm nf} - k_{\rm Cu})} \times (k_{\rm nf}) \text{ where } k_{\rm nf} = \frac{k_{\rm Al_2O_3} + 2k_{\rm f} - 2\phi_{\rm Al_2O_3}(k_{\rm f} - k_{\rm Al_2O_3})}{k_{\rm Al_2O_3} + 2k_{\rm f} + \phi_{\rm Al_2O_3}(k_{\rm f} - k_{\rm Al_2O_3})} \times (k_{\rm f})$
Heat capacity	$(\rho c_{\rm p})_{\rm hnf}/(\rho c_{\rm p})_{\rm f} = (1-\phi_{\rm Cu})[(1-\phi_{\rm Al_2O_3})+\phi_{\rm Al_2O_3}(\rho c_{\rm p})_{\rm Al_2O_3}/(\rho c_{\rm p})_{\rm f}]$
	+ $\phi_{ m Cu}( ho c_{ m p})_{ m Cu}/( ho c_{ m p})_{ m f}$

transformation that simplifies complex flow equations by reducing the dependent and independent variables. The following ordinary differential equations (ODEs) are obtained:

$$\frac{\mu_{\rm nf}/\mu_{\rm f}}{\rho_{\rm nf}/\rho_{\rm f}} \left\{ 1 + \frac{1}{\beta} \right\} \left\{ \eta f''' + f'' \right\} + \left\{ f f'' - f'^2 + 1 \right\} = 0, \quad (6)$$

$$\frac{(k_{\rm nf}/k_{\rm f})}{\Pr(\rho c_{\rm p})_{\rm nf}/(\rho c_{\rm p})_{\rm f}} \{\eta \theta'' + \theta'\} + \operatorname{Re} f \theta' = 0. \tag{7}$$

Boundary conditions are as follows:

$$\begin{cases} f(1) = 0, f'(1) = \lambda, \theta(1) = 1\\ f'(\eta) \to 1, \theta(\eta) \to 0 \text{ as } \eta \to \infty \end{cases}$$
(8)

where (′) represents the differentiation with respect to  $\eta$ , and  $\mathrm{Re} = \frac{ca^2}{2\vartheta_\mathrm{f}}$  and  $\mathrm{Pr} = \frac{\mu_\mathrm{f}(c_\mathrm{p})_\mathrm{f}}{k_\mathrm{f}}$  are the Reynolds and Prandtl numbers, respectively. Furthermore, the stretching/shrinking parameter is  $\lambda = \frac{b}{c}$ , and the static cylinder is represented by the value  $\lambda = 0$ ,  $\lambda > 0$  for stretching, and  $\lambda < 0$  for shrinking cylinder.

Furthermore, the physical quantities skin friction coefficient  $C_{\rm f}$  and the local Nusselt number Nu are represented as follows:

$$C_{\rm f} = \frac{2\mu_{\rm hnf}}{\rho_{\rm f} w_{\rm e}^2} \left[ 1 + \frac{1}{\beta} \left| \left( \frac{\partial w}{\partial r} \right)_{r=a} \right|, \text{ and} \right]$$

$$Nu = -\frac{ak_{\rm hnf}}{k_{\rm f} (T_{\rm w} - T_{\infty})} \left( \frac{\partial T}{\partial y} \right)_{r=a}$$
(9)

Substituting equation (5) into equation (9), we have

$$\left(\frac{\text{Rez}}{a}\right)C_{\text{f}} = \mu_{\text{hnf}}/\mu_{\text{f}}\left(1 + \frac{1}{\beta}\right)f''(1); \text{Nu} = -2\frac{k_{\text{hnf}}}{k_{\text{f}}}\theta'(1).$$
 (10)

# 3 Results and discussion

The bvp4c technique, which runs on the MATLAB program, is used to numerically assess the framework of higher-

order nonlinear ODEs as specified in equations (6) and (7) through the boundary conditions in equation (8). The three-stage Lobatto IIIA algorithm is implemented by the bvp4c solver with finite difference method; as a result, the temperature and velocity distributions asymptotically fulfilled the boundary requirement. The results are then precise to the fourth order in terms of numbers. Several initial estimations for  $\left(\frac{\text{Re}z}{a}\right) C_{\mathrm{f}}$  and Nu were used to create the first solution and second solution in Figures 11-14. In addition, the current numerical values of  $\left(\frac{\text{Re}z}{a}\right)C_{\mathrm{f}}$  and Nu under several applied parameters when Pr = 7 and Re = 2are presented in Table 3. The most current results are verified by referring to data from earlier studies to verify the accuracy of the technique. Furthermore, the comparison amounts of f''(1) are assessed in Table 4 based on the conclusions of Wang [25], Wang [26], and Waini et al. [33]. The correlation has been observed to be in perfect agreement with the literature that was referenced, which confirmed that the current numerical findings are accurate.

The effects of velocity  $f'(\eta)$  and temperature  $\theta(\eta)$  profiles are illustrated in Figures 2–10 correspondingly. Figures 2 and 3 represent the existence of several

**Table 4:** Comparison of f''(1) values under various values of Re when  $\beta=\infty, \lambda=0, \phi_{\text{Cu}}=0$ , and  $\phi_{\text{Al}_2\text{O}_3}=0$ 

Re	Current results	Wang [25] <i>f</i> "(1)	Wang [26]	Waini <i>et al.</i> [33]
0.2	0.786042	0.78605	0.78604	0.786042
1	1.48420664	1.484185	1.48418	1.484183
2	2.00000005	_	_	_
4	2.72621056	_	_	_
6	3.28224202	_	_	_
8	3.75055319	_	_	_
10	4.162919748	4.16292	4.16292	4.162920

**Table 3:** Current numerical values of  $\left(\frac{\text{Rez}}{a}\right)C_f$  and Nu under various applied parameters when Pr=7 and Re=2

$\varphi_{Al_2O_3}$	$\varphi_{Cu}$	β	–λ	1st solution $\left(rac{ ext{Rez}}{a} ight)\!C_{ ext{f}}$	2nd solution	1st solution Nu	2nd solution
0.04	0			2.967921	-0.18825	0.187871	1.0 × 10 <sup>-15</sup>
	0.04			3.450883	-0.19549	0.355184	$4.73 \times 10^{-12}$
	0.1	5		4.227721	-0.21482	0.661377	$6.83 \times 10^{-9}$
	0.04	10		3.256991	-0.17121	0.404754	$4.277 \times 10^{-11}$
		∞	1.2	3.057848	-0.14691	0.463336	$3.92 \times 10^{-10}$
			1.25	2.925761	-0.05926	0.329031	$8.84 \times 10^{-9}$
			1.3	2.759202	0.070803	0.213295	$1.34 \times 10^{-7}$

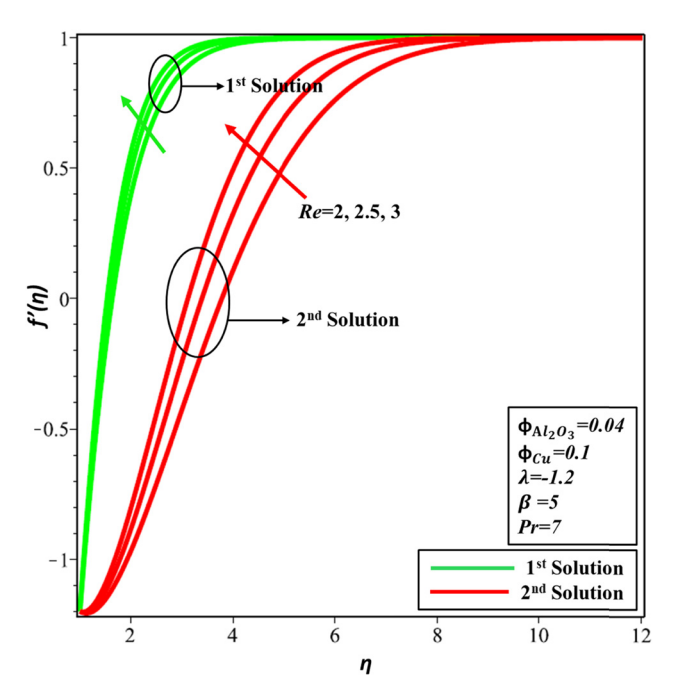


**Figure 2:** Behavior of  $f'(\eta)$  profile against different values of Re.

parameter values, such as  $\phi_{\text{Al}_2\text{O}_3}$  = 0.04,  $\phi_{\text{Cu}}$  = 0.1,  $\lambda$  = -1.2,  $\beta$  = 5, and Pr = 7 alongside three fixed quantities of Re = 2, 2.5, and 3. In this study, Re = 2, 2.5, and 3 ranges are considered. The values used for Re in Figures 2 and 3 are between the ranges of values that are  $0.5 \le \text{Re} \le 100$ , which met the boundary condition  $\eta \to \infty$  asymptotically and produced dual solutions, under the recommendation given by Lok and Pop [32]. In Figure 2, velocity profile  $f'(\eta)$ behavior increased, while in Figure 3, temperature profile  $\theta(\eta)$  behavior declined in both solutions as the quantity of Re parameters enhanced. Physically, the flow tends to grow more turbulent as the Re rises, and the velocity  $f'(\eta)$  profile shifts to show increased velocity along the edges and a flatter profile in the middle. This behavior, which is typical of turbulent flows, is brought on by the fluid's increased mixing and chaotic motion. Therefore, after thermal diffusion is weakened, the temperature  $\theta(\eta)$  profile drops. This finding yields comparable outcomes to those reported by Lok and Pop [32] for viscous fluid.

Figures 4 and 5 demonstrate the velocity  $f'(\eta)$  and temperature  $\theta(\eta)$  profiles against the influence of the shrinking parameter  $\lambda=-1.2,-1.3,$  and -1.4 with various parameters, including  $\phi_{\text{Al}_2\text{O}_3}=0.04,$   $\phi_{\text{Cu}}=0.1,$  Re =2,  $\beta=5,$  and Pr = 7. This range was chosen because Lok and Pop [32] suggested that the values for the shrinkage parameter in Figures 4 and 5 ought to lie between -1.0 and -1.5. This range of  $\lambda \in [-1.2 \text{ to } -1.4]$  satisfied the boundary condition. Figure 4 revealed that first solution of  $f'(\eta)$  is declined and the second solution is enhanced when the amount of

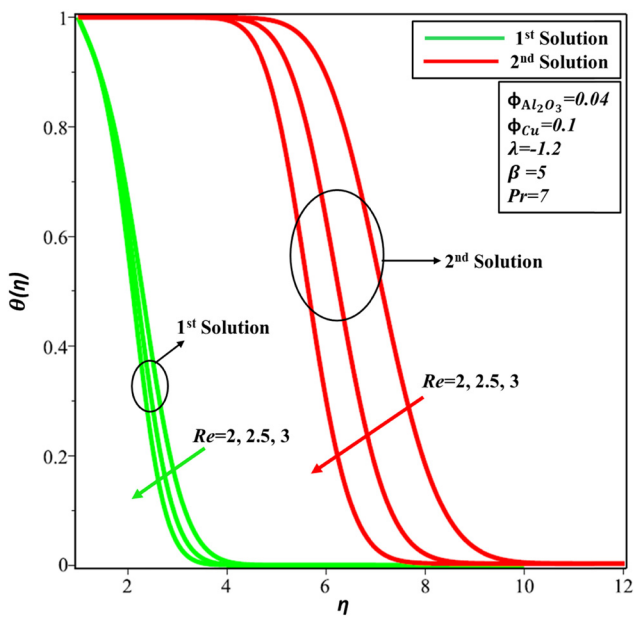


**Figure 3:** Behavior of  $\theta(\eta)$  profile against different values of Re.

shrinking parameter  $\lambda$ upsurges, although in Figure 5 for  $\theta(\eta)$ , the opposite trend can be seen in both solutions, respectively. Physically, the hybrid nanofluid's nanoparticles can also change the way fluid flows close to the surface. As an instance, they might lower fluid velocity close to the surface, which would raise shear stress and raise the velocity  $f'(\eta)$  profile. When the parameter of shrinking surface increases in a hybrid nanofluid system, the temperature

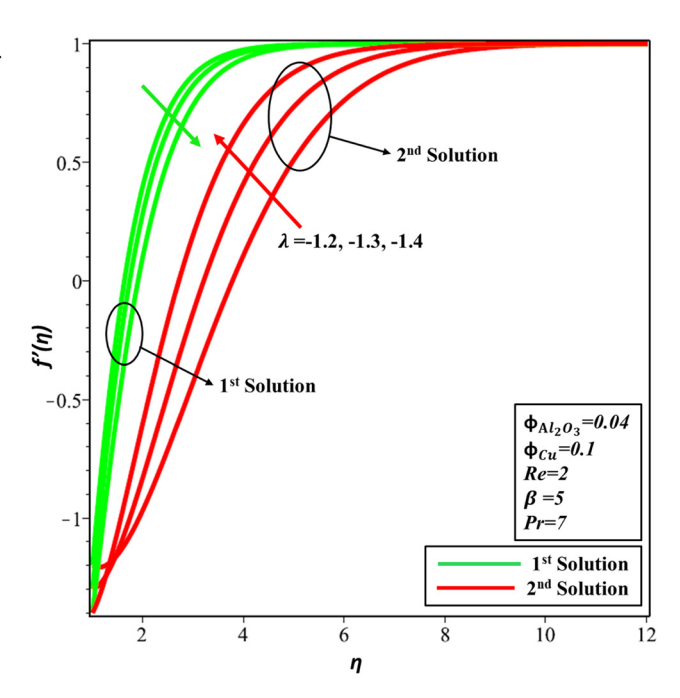
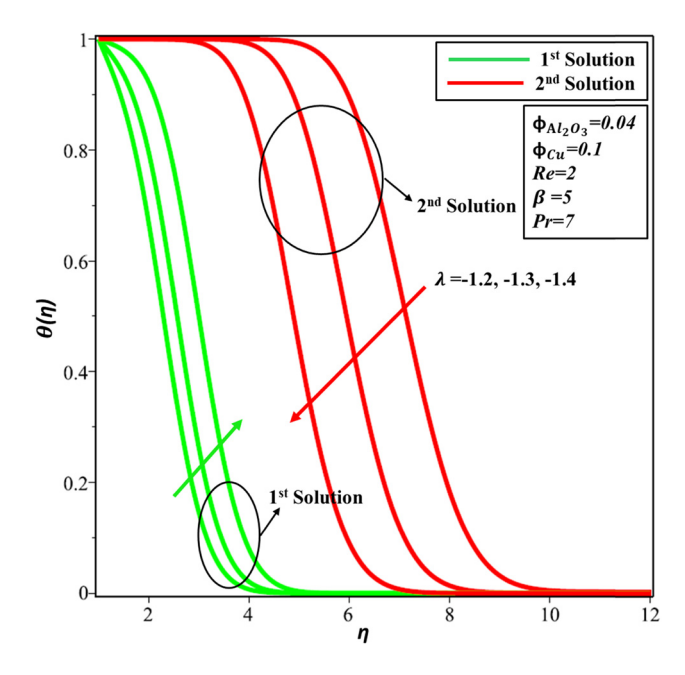


**Figure 4:** Variation of  $f(\eta)$  for different values of  $\lambda$ .





 $\theta(\eta)$  profile tends to decrease due to changes in the boundary-layer thickness, altered nanoparticle dispersion, and increased conductive heat transfer across the boundary layer. These findings were corroborated by Waini *et al.* [33].

Figures 6 and 7 highlight the velocity  $f'(\eta)$  and temperature  $\theta(\eta)$  profiles against the impact of Casson fluid parameter  $\beta$  = 5, 10, and $\infty$  against  $\eta$  for a variety of parameters, as well as including  $\phi_{\text{Al}_2\text{O}_3}$  = 0.04,  $\phi_{\text{Cu}}$  = 0.1, Re = 2,

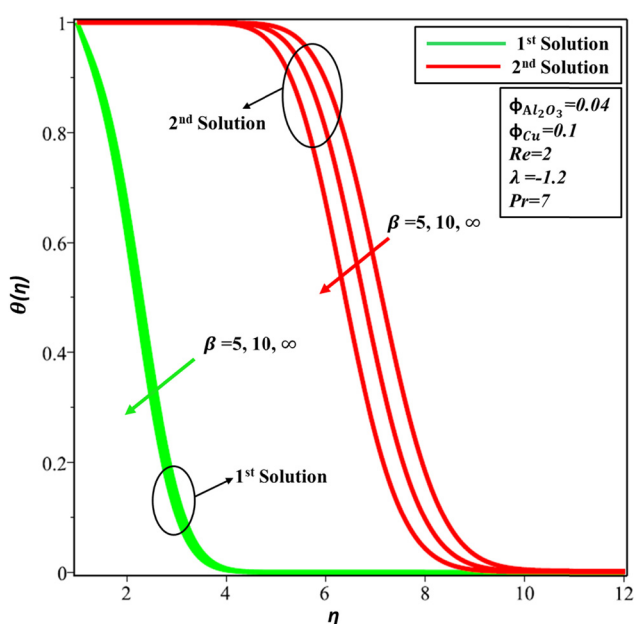


**Figure 7:** Variation of  $\theta(\eta)$  profiles for different values of  $\beta$ .

 $\lambda=-1.2$ , and  $\Pr=7$ . The Casson fluid parameter  $\beta\in[1-\infty]$  was used by Mousavi *et al.* [39] in their study, and this collection  $\beta\in[5-\infty]$  is implemented in Figures 6 and 7 to satisfy the boundary conditions. When the Casson fluid parameters were enhanced as shown in Figure 6, the velocity profile  $f'(\eta)$  in both solutions increased. On the other hand, as the value of the Casson fluid parameter increased in Figure 7, the thermal thickness decreased in both solutions. The SA–hybrid nanofluid flow

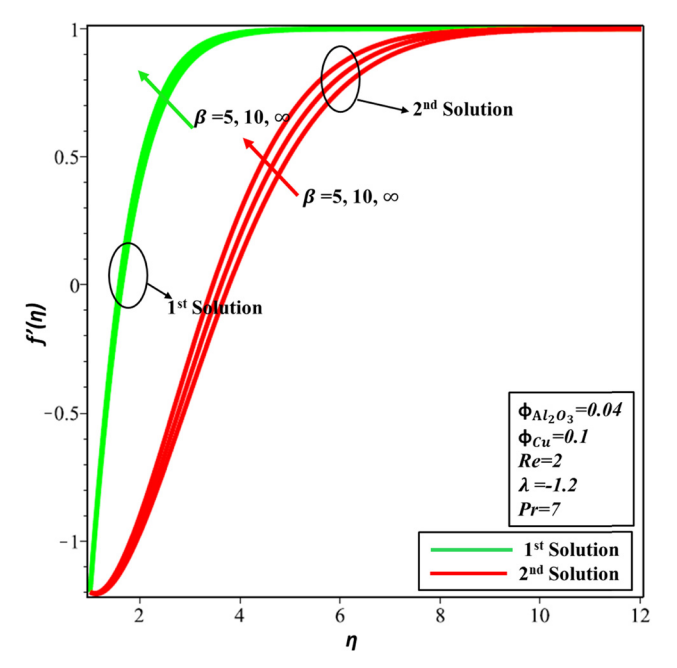


**Figure 6:** Variation of  $f'(\eta)$  profiles for different values of  $\beta$ .

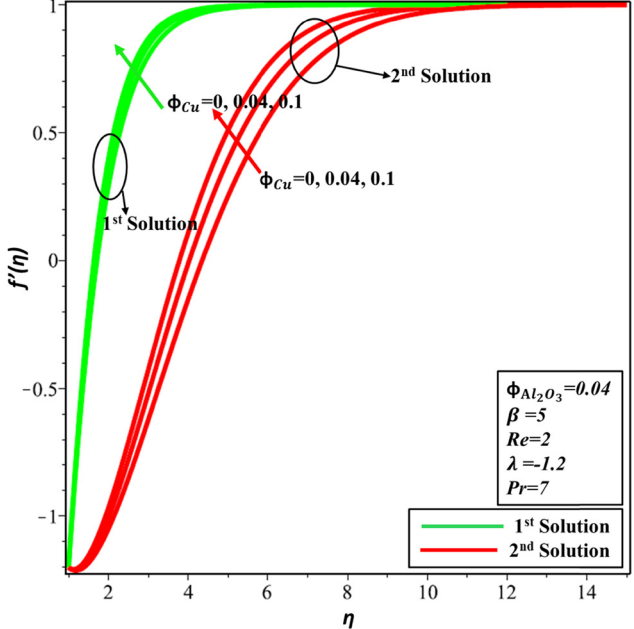


**Figure 8:** Variation of  $f'(\eta)$  profiles for various values of  $\phi_{\mathrm{Cu}}$ .

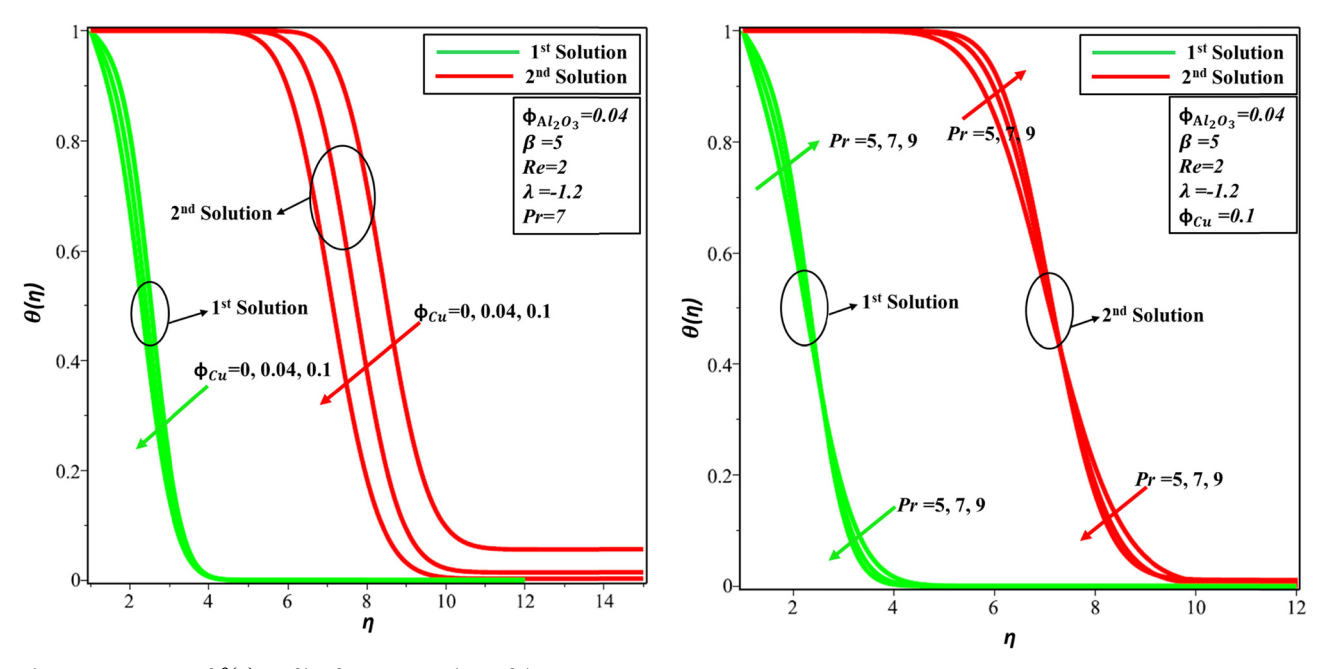


**Figure 9:** Variation of  $\theta(\eta)$  profiles for various values of  $\phi_{\mathrm{Cu}}$ .

**Figure 10:** Variation of  $\theta(\eta)$  profiles for various values of Pr.

experiences a physically higher viscous force, leading to a reduction in  $\theta(\eta)$  profile. Physically, when the Casson fluid parameter increases, the fluid becomes more resistant to deformation and flow. This could result in a reduction in the fluid's effective heat transfer coefficient, leading to a decrease in the convective heat transfer rate and, consequently, a lower temperature profile.

Plots of velocity  $f'(\eta)$  and temperature  $\theta(\eta)$  profiles against solid volume fraction  $\phi_{\rm Cu}$  = 0, 0.04, and 0.1 with different parameter  $\phi_{\rm Al_2O_3}$  = 0.04,  $\beta$  = 5, Re = 2,  $\lambda$  = -1.2,

and Pr = 7 are displayed in Figures 8 and 9, respectively. Hammachukiattikul *et al.* [20] employed a range of  $\phi_{\text{Cu}}$  (0.05  $\leq \phi_{\text{Cu}} \leq$  0.2) in their study. This range is in the set of ranges (0.0  $\leq \phi_{\text{Cu}} \leq$  0.1), which is used in Figures 8 and 9 to meet the boundary conditions. Figure 8 illustrates that the momentum wall surface stiffness increases in both solutions as the value of  $\phi_{\text{Cu}}$  grows, but in Figure 9, both solutions are decreased. Therefore, thermal boundary

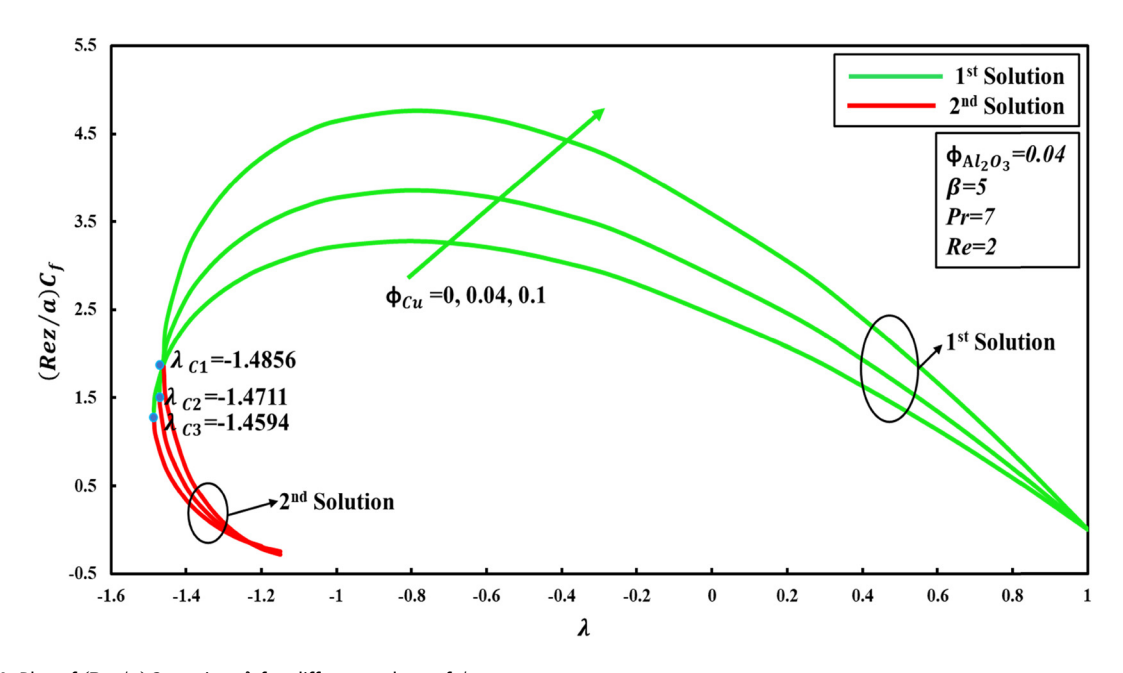


**Figure 11:** Plot of  $(\text{Rez}/a)\mathcal{C}_{\mathrm{f}}$  against  $\lambda$  for different values of  $\phi_{\mathrm{Cu}}$ .

8 — Mustafa Abbas Fadhel et al. DE GRUYTER

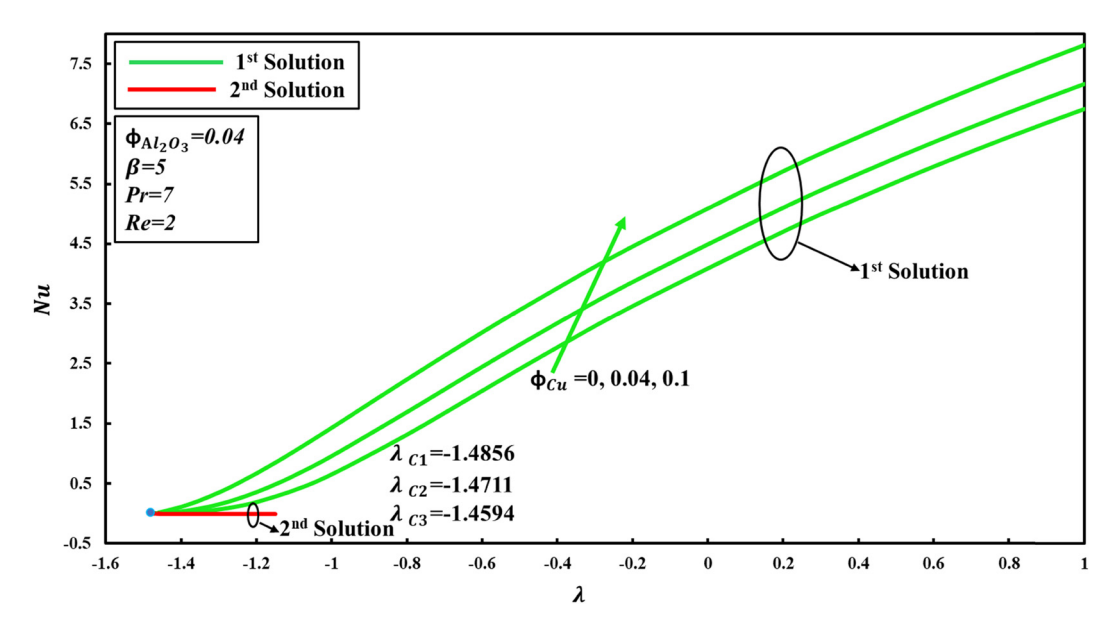


**Figure 12:** Plot of Nu against  $\lambda$  for different values of  $\phi_{\mathrm{Cu}}$ .

surface thickness declined in both solutions. Physically, it indicates that the enclosing quantity of a solid volume fraction can slow down the SA-based hybrid nanofluid movement. Research carried out by Waini *et al.* [33] lent support to the conclusions presented here. In addition, the second solution does not converge properly and satisfy boundary conditions, indicating that this model is weaker for nanofluid than for hybrid nanofluid and that there are no multiple solutions for nanofluid cases.

Figure 10 shows the temperature profile  $\theta(\eta)$  for the Prandtl number  $\Pr = 5, 7$ , and 9 with various values, such as  $\phi_{\text{Al}_2\text{O}_3} = 0.04$ ,  $\phi_{\text{Cu}} = 0.1$ ,  $\beta = 5$ , Re = 2, and  $\lambda = -1.2$ , respectively. Hammachukiattikul *et al.* [20] used a variety of different  $\Pr$  values, ranging from 0.72 to 100 in their research. This range is included in this set of ranges  $(5 \le \Pr \le 9)$ , as shown in Figure 10, to fulfill the boundary conditions. Thermal thickness upsurged in both solutions, but then the opposite trend behavior appears  $(\theta(\eta) < 0.04)$ .

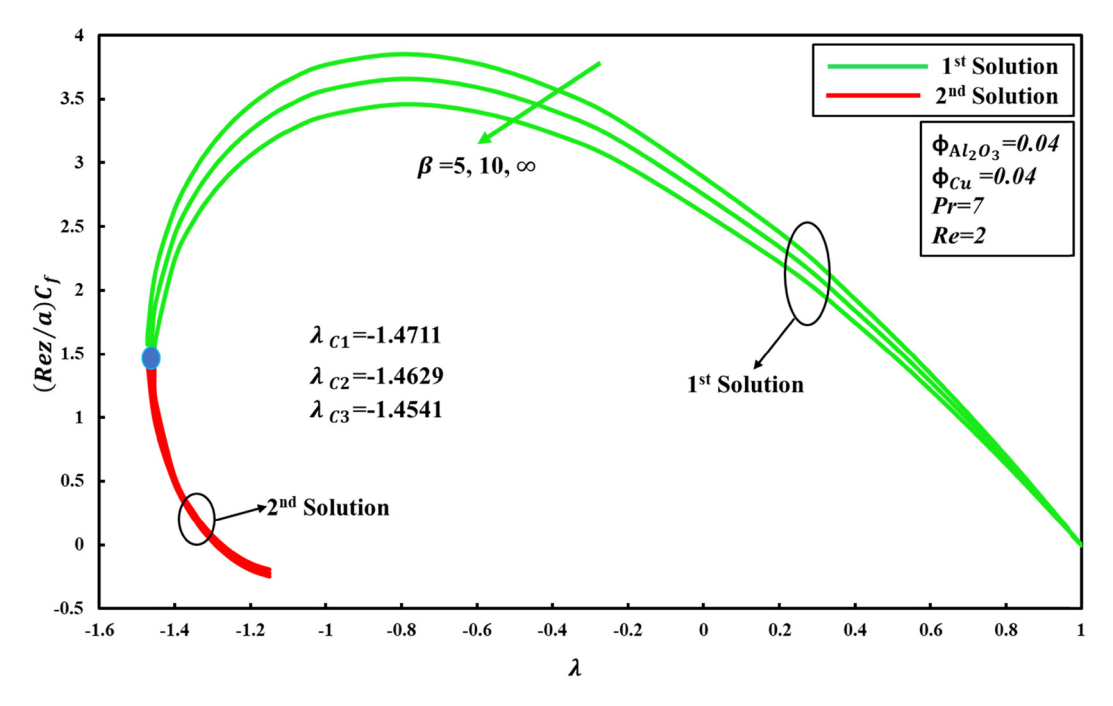


**Figure 13:** Plot of  $(\text{Rez}/a)C_f$  against  $\lambda$  for different values of  $\beta$ .

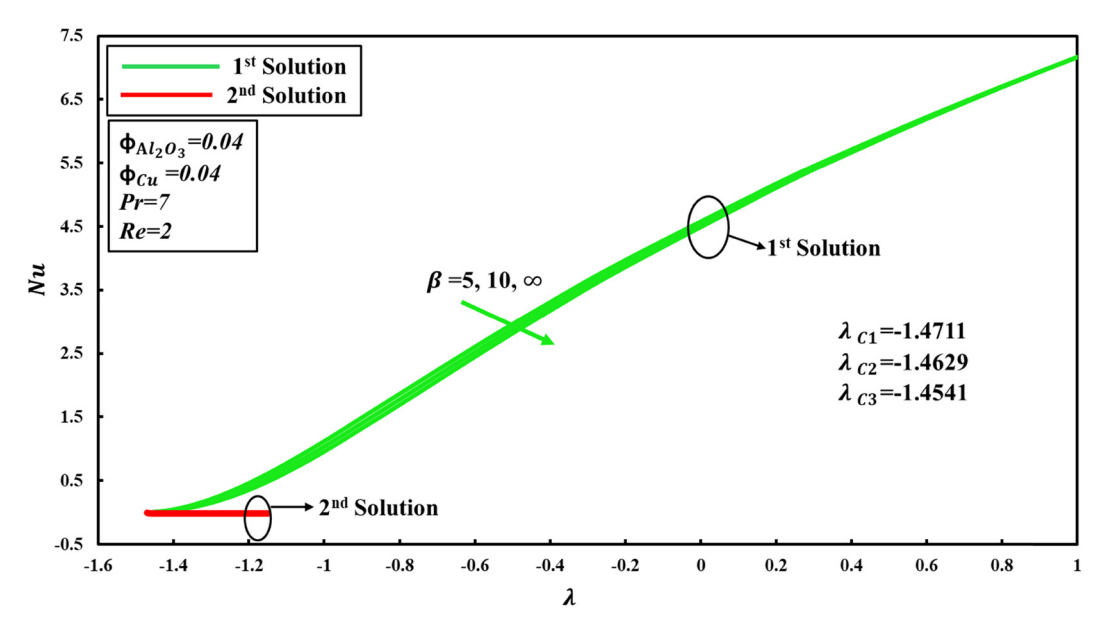


**Figure 14:** Plot of Nu against  $\lambda$  for different values of  $\beta$ .

Physically, the fluid's thermal diffusivity is comparatively less than its momentum diffusivity when the Prandtl number Pr is raised. In other words, the fluid is better at transferring heat than it is at transferring momentum.

As shown in Figures 11-14, the non-uniqueness of the solutions to equations (6)–(8) is observed for some different quantities of the parameter. The variation of  $\left(\frac{\text{Rez}}{a}\right) C_{\text{f}}$ and Nu is demonstrated in Figures 11 and 12 by the occurrence of several parameter quantities incorporating  $\phi_{\text{Al}_2\text{O}_3}$  = 0.04,  $\beta$  = 5, Re = 2, and Pr = 7 with three fixed quantities of the solid volume fraction copper  $\phi_{\mathrm{Cu}}$  = 0, 0.04, and 0.1 against  $\lambda$ . Dual solutions for  $\lambda_c < \lambda < -1.2$ are feasible. Furthermore, unique solution is observed when  $\lambda \geq -1.2$ , and whenever  $\lambda < \lambda_{ci}$ , there is no possible solution.  $\lambda_{ci}$  is the critical point of  $\lambda$ , since it is the connection point between the first solution and the second solution. It is important to note that as  $\phi_{Cu} = 0$ , the value formed for  $\lambda_{c1} = -1.4856$ , after that, 4% of  $\phi_{Cu}$  being included in the hybrid nanofluid, and value of  $\lambda_{c2} = -1.4711$ . In addition, the amount of  $\lambda_{c3} = -1.4594$  appeared to augment as 10% of the volume fraction of  $\phi_{\text{Cu}}$  being included in the hybrid nanofluid. Figure 11 demonstrates that skin friction  $\left(\frac{\text{Rez}}{a}\right)C_{\text{f}}$ increased as the amount of solid nanoparticle  $\phi_{\mathrm{Cu}}$  increased.

increased as the amount of solid nanoparticle  $\phi_{\text{Cu}}$  increased. A similar behavior is noted in Figure 12 for Nusselt number Nu as the quantity of  $\phi_{\text{Cu}}$  increased. Physically, when assessing the three kinds of fluid, it is revealed that hybrid nanofluid has higher physical quantities compared to all of them. The finding is in agreement with the premise that the addition of hybrid nanoparticles,

which are capable of producing synergistic influences, can increase the heat transfer rate. Similar findings were found by Waini *et al.* [33].

Figures 13 and 14 demonstrate the variation of  $\left(\frac{\text{Rez}}{a}\right)C_{\text{f}}$ and Nu with several parameter quantities such as  $\phi_{\text{Al}_2\text{O}_3}$  = 0.04,  $\phi_{\text{Cu}}$  = 0.04, Pr = 7, and Re = 2 with three set quantities of the Casson fluid parameter  $\beta$  = 5, 10, and  $\infty$ against shrinking parameter  $\lambda$ . It is stated that dual solutions for  $\lambda_{ci} < \lambda < -1.2$  are possible. Additionally, when  $\lambda < \lambda_{ci}$ , there is no possible solution that happens, and a sole solution is perceived when  $\lambda \ge -1.2$ .  $\lambda_{ci}$ , i = 1,2,3 is the critical point of  $\lambda$ , since it is the interaction point between the first solution and the second solution. It is seen that as  $\beta$  = 5, the value generated for  $\lambda_{c1}$  = -1.4711; later, Casson quantity enhanced when  $\beta = 10$  the amount attained for  $\lambda_{c2} = -1.4629$ . In addition, the quantity of  $\lambda_{c3} = -1.4541$ happened as the quantity of the Casson parameter  $\beta = \infty$ occurred in the SA-hybrid nanofluid. Figure 13 illustrates that skin friction  $\left(\frac{\text{Rez}}{a}\right)C_{\text{f}}$  declined as the quantity of Casson parameter  $\beta$  intensified. The same behavior is found in Figure 14 for Nusselt number Nu as the quantity of Casson parameter  $\beta$  improved. A physically greater viscous force occurs on the SA-hybrid nanofluid flow, resulting in a reduction in  $\left|\frac{\text{Rez}}{a}\right| C_{\text{f}}$  and Nu. Higher Casson fluid parameters can improve the fluid's thermal conductivity properties by making it behave more like a solid at rest. As a result, the fluid's ability to transmit heat increases, making it easier to move heat from hotter to cooler areas.

# 4 Conclusion

The Casson SA-hybrid nanofluid flow toward a stagnation point on a stretching/shrinking cylinder has been observed in the current study. The outcomes have been found by using the bvp4c algorithm that is included in the Matlab program. Validation of the findings was carried out for those specific instances in which it was found that the latest findings were compared favorably with the preceding findings. This study accounts for the Reynolds number, shrinking surface, Casson fluid, the solid volume fraction of copper, and the Prandtl number as parameters that are present in behavior of temperature and velocity profiles. Furthermore, the Casson fluid parameters and copper solid volume fraction against shrinking parameter for the skin friction coefficient and the Nusselt number were also examined in this study. The following are some of the inferences that can be made:

- Based on the findings of the study, the existence of hybrid nanoparticles led to an upsurge in the rate of heat transfer.
- 2) The specific physical features allow for the possibility of dual solutions, with the categorization of the solutions taking place in the shrinking zone ( $\lambda$  < 0).
- 3) The rate of heat transport declined in both solutions as the quantity of Reynold's number, Casson fluid, and solid volume fraction parameters increased.
- 4) Thermal boundary-layer thickness of Pr number upsurged in both solutions, while declined behavior was then noted when  $\theta(\eta) < 0.04$ .
- 5) The Nusselt Nu number decreased as the amount of Casson SA–hybrid nanofluid increased.

This study is limited to polar coordinates of a cylinder with SA-hybrid nanofluid toward a stagnation point flow over stretching/shrinking with the effect of Casson fluid. Additionally, this study can be extended to two-dimensional Cartesian coordinate hybrid ferrofluid flow with several effects such as thermal radiation, viscous dissipation, and convective boundary condition.

**Acknowledgments:** The authors extend their appreciation to the Deanship of Scientific Research at King Khalid University Abha 61421, Asir, Kingdom of Saudi Arabia for funding this work through the Small Groups Project under the grant number RGP.1/427/44.

**Funding information:** This project was financially supported by Lucian Blaga University of Sibiu through research grant LBUS-IRG-2023-09.

**Author contributions:** All authors have accepted responsibility for the entire content of this manuscript and approved its submission.

**Conflict of interest:** The authors state no conflict of interest.

**Data availability statement:** The datasets generated and/ or analyzed during the current study are available from the corresponding author on a reasonable request.

# References

- [1] Barnoon P, Toghraie D, Eslami F, Mehmandoust B. Entropy generation analysis of different nanofluid flows in the space between two concentric horizontal pipes in the presence of magnetic field: single-phase and two-phase approaches. Computers Math Appl. 2019;77(3):662–92.
- [2] Zubair T, Usman M, Hamid M, Sohail M, Nazir U, Nisar KS, et al. Computational analysis of radiative Williamson hybrid nanofluid comprising variable thermal conductivity. Jpn J Appl Phys. 2021;60(8):087004.
- [3] Asghar A, Lund LA, Shah Z, Vrinceanu N, Deebani W, Shutaywi M. Effect of thermal radiation on three-dimensional magnetized rotating flow of a hybrid nanofluid. Nanomaterials. 2022:12(9):1566.
- [4] Farhan M, Omar Z, Mebarek-Oudina F, Raza J, Shah Z, Choudhari RV, et al. Implementation of the one-step one-hybrid block method on the nonlinear equation of a circular sector oscillator. Comput Math Model. 2020;31:116–32.
- [5] Asghar A, Chandio AF, Shah Z, Vrinceanu N, Deebani W, Shutaywi M, et al. Magnetized mixed convection hybrid nanofluid with effect of heat generation/absorption and velocity slip condition. Heliyon. 2023;9(2):e13189.
- [6] Saeed A, Bilal M, Gul T, Kumam P, Khan A, Sohail M. Fractional order stagnation point flow of the hybrid nanofluid towards a stretching sheet. Sci Rep. 2021;11(1):20429.
- [7] Abo-Dahab SM, Abdelhafez MA, Mebarek-Oudina F, Bilal SM. MHD Casson nanofluid flow over nonlinearly heated porous medium in presence of extending surface effect with suction/injection. Indian J Phys. 2021;95(12):1–15.
- [8] Asghar A, Vrinceanu N, Ying TY, Lund LA, Shah Z, Tirth V. Dual solutions of convective rotating flow of three-dimensional hybrid nanofluid across the linear stretching/shrinking sheet. Alex Eng J. 2023:75:297–312.
- [9] Hayat T, Nadeem S. Heat transfer enhancement with Ag-CuO/ water hybrid nanofluid. Results Phys. 2017;7:2317-24.
- [10] Waini I, Ishak A, Groşan T, Pop I. Mixed convection of a hybrid nanofluid flow along a vertical surface embedded in a porous medium. Int Commun Heat Mass Transf. 2020;114:104565.
- [11] Gholinia M, Armin M, Ranjbar AA, Ganji DD. Numerical thermal study on CNTs/C<sub>2</sub>H<sub>6</sub>O<sub>2</sub>–H<sub>2</sub>O hybrid base nanofluid upon a porous stretching cylinder under impact of magnetic source. Case Stud Therm Eng. 2019;14:100490.
- [12] Swain K, Mebarek-Oudina F, Abo-Dahab SM. Influence of MWCNT/  $Fe_3O_4$  hybrid nanoparticles on an exponentially porous shrinking

- sheet with chemical reaction and slip boundary conditions. J Therm Anal Calorim. 2022;147(2):1561–70.
- [13] Asghar A, Ying TY, Zaimi WMKAW. Two-dimensional mixed convection and radiative Al<sub>2</sub>O<sub>3</sub>-Cu/H<sub>2</sub>O hybrid nanofluid flow over a vertical exponentially shrinking sheet with partial slip conditions. CFD Lett. 2022;14(3):22–38.
- [14] Lund LA, Omar Z, Khan I. Darcy-Forchheimer porous medium effect on rotating hybrid nanofluid on a linear shrinking/stretching sheet. Int | Numer Methods Heat Fluid Flow. 2021;31(12):3621–41.
- [15] Sajjad M, Mujtaba A, Asghar A, Ying TY. Dual solutions of magnetohydrodynamics  $Al_2O_3$  + Cu hybrid nanofluid over a vertical exponentially shrinking sheet by presences of joule heating and thermal slip condition. CFD Lett. 2022;14(8):100–15.
- [16] Dero S, Shaikh H, Talpur GH, Khan I, Alharbim SO, Andualem M. Influence of a Darcy-Forchheimer porous medium on the flow of a radiative magnetized rotating hybrid nanofluid over a shrinking surface. Sci Rep. 2021;11(1):24257.
- [17] Hatami M, Ganji DD. Heat transfer and flow analysis for SA-TiO<sub>2</sub> non-Newtonian nanofluid passing through the porous media between two coaxial cylinders. J Mol Liq. 2013;188:155–61.
- [18] Akinshilo AT, Olofinkua JO, Olaye O. Flow and heat transfer analysis of the sodium alginate conveying copper nanoparticles between two parallel plates. J Appl Comput Mech. 2017;3(4):258–66.
- [19] Hussanan A, Qasim M, Chen ZM. Heat transfer enhancement in sodium alginate based magnetic and non-magnetic nanoparticles mixture hybrid nanofluid. Phys A: Stat Mech Appl. 2020;550:123957.
- [20] Hammachukiattikul P, Govindaraju M, Sohail M, Vadivel R, Gunasekaran N, Askar S. Analytical study on sodium alginate-based hybrid nanofluid flow through a shrinking/stretching sheet with radiation, heat source and inclined Lorentz force effects. Fractal Fract. 2022;6(2):68.
- [21] Dawar A, Said NM, Islam S, Shah Z, Mahmuod SR, Wakif A. A semianalytical passive strategy to examine a magnetized heterogeneous mixture having sodium alginate liquid with alumina and copper nanomaterials near a convectively heated surface of a stretching curved geometry. Int Commun Heat Mass Transf. 2022;139:106452.
- [22] Khan U, Mebarek-Oudina F, Zaib A, Ishak A, Abu Bakar S, Sherif ESM, et al. An exact solution of a Casson fluid flow induced by dust particles with hybrid nanofluid over a stretching sheet subject to Lorentz forces. Waves Random Complex Media. 2022;1–14.
- [23] Dawar A, Islam S, Shah Z, Lone SA. A comparative analysis of the magnetized sodium alginate-based hybrid nanofluid flows through cone, wedge, and plate. ZAMM-J Appl Math Mech/Zeitschrift für Angew Mathematik und Mechanik. 2023;103(1):e202200128.

- [24] Raza J, Mebarek-Oudina F, Lund LA. The flow of magnetised convective Casson liquid via a porous channel with shrinking and stationary walls. Pramana J Phys. 2020;2022(96):229.
- [25] Wang CY. Axisymmetric stagnation flow on a cylinder. Q Appl Math. 1974;32(2):207–13.
- [26] Wang CY. Stagnation flow on a cylinder with partial slip—an exact solution of the Navier–Stokes equations. IMA J Appl Math. 2007;72(3):271–7.
- [27] Reddy Gorla RS. Heat transfer in an axisymmetric stagnation flow on a cylinder. Appl Sci Res. 1976;32:541–53.
- [28] Merkin JH, Najib N, Bachok N, Ishak A, Pop I. Stagnation-point flow and heat transfer over an exponentially stretching/shrinking cylinder. J Taiwan Inst Chem Eng. 2017;74:65–72.
- [29] Zaimi WW, Ishak A, Pop I. Unsteady viscous flow over a shrinking cylinder. J King Saud Univ-Sci. 2013;25(2):143–8.
- [30] Cunning GM, Davis AMJ, Weidman PD. Radial stagnation flow on a rotating circular cylinder with uniform transpiration. J Eng Math. 1998;33:113–28.
- [31] Soomro FA, Zaib A, Haq RU, Sheikholeslami M. Dual nature solution of water functionalized copper nanoparticles along a permeable shrinking cylinder: FDM approach. Int J Heat Mass Transf. 2019;129:1242–9.
- [32] Lok YY, Pop I. Wang's shrinking cylinder problem with suction near a stagnation point. Phys Fluids. 2011;23(8):083102.
- [33] Waini I, Ishak A, Pop I. Hybrid nanofluid flow towards a stagnation point on a stretching/shrinking cylinder. Sci Rep. 2020;10(1):1–12.
- [34] Pandey AK, Kumar M. Boundary layer flow and heat transfer analysis on Cu-water nanofluid flow over a stretching cylinder with slip. Alex Eng J. 2017;56(4):671–7.
- [35] Abbas N, Nadeem S, Saleem A, Malik MY, Issakhov A, Alharbi FM. Models base study of inclined MHD of hybrid nanofluid flow over nonlinear stretching cylinder. Chin J Phys. 2021;69:109–17.
- [36] Iorgoaiea Guignard M, Campagne C, Giraud S, Brebu M, Vrinceanu N, Cioca LI. Functionalization of a bamboo knitted fabric using air plasma treatment for the improvement of microcapsules embedding. J Text Inst. 2015;106(2):119–32. WOS:000345570900002.
- [37] Popovici RF, Alexa IF, Novac O, Vrinceanu N, Popovici E, Lupusoru CE, et al. Pharmacokinetics study on mesoporous silicacaptopril controlled release systems. Dig J Nanomater Biostruct. 2011;6(3):1619–30WOS:000300568100018.
- [38] Zainal NA, Nazar R, Naganthran K, Pop I. Unsteady MHD hybrid nanofluid flow towards a horizontal cylinder. Int Commun Heat Mass Transf. 2022;134:106020.
- [39] Mousavi SM, Rostami MN, Yousefi M, Dinarvand S, Pop I, Sheremet MA. Dual solutions for Casson hybrid nanofluid flow due to a stretching/shrinking sheet: A new combination of theoretical and experimental models. Chin J Phys, 2021;71:574–88.